The stages that constitute the proposed algorithm are illustrated in the block diagram shown in fig. 1. For each variable density under-sampled k-space acquisition, a fixed number of low-frequency rows at the centre of the k-space plus an equal number of evenly spaced high-frequency rows are captured. For example, to sample 50% (32 rows) of the k-space of a 64×32 pixels image, 16 rows are obtained from the centre of the k-space (rows 25 to 40). The other 16 rows (1, 4, 7, 10, 13, 16, 19, 22, 43, 46, 49, 52, 55, 58, 61 and 64) are selected to be evenly selected from either side of the picked central rows. This acquisition paradigm can be modelled as an element-wise product of the full k-space $\boldsymbol{S}(u,v)$ and a variable-density mask as;

$$\boldsymbol{S_u^{'}}(u,v) = \boldsymbol{S}(u,v).\boldsymbol{\mathcal{M}}(u,v) \quad (13)$$

where $\boldsymbol{S_u^{'}}(u,v)$ is the under-sampled k-space and $\boldsymbol{\mathcal{M}}(u,v)$ is a proposed mask given by;

$$\boldsymbol{\mathcal{M}}(u,v) = \begin{cases} 1 \quad \text{for } v \geq v_1\,, v \leq v_2 \text{ where } v_2 > v_1 \\ 0 \text{ for } v < v_1,\ v > v_2 \text{ and } \mathrm{mod}(v,q) = 0 \\ 0 \quad \text{elsewhere} \end{cases} \quad (14)$$

where $v \in (1,\ N_p)$, $u \in (1,\ N_r)$ and N_r is the number of read-out gradient steps [13]. For each measurement, the values of integers v_1, v_2 and q are selected to achieve the desired percentage measurement. For a 50% under-sampling, $v_1 = 25$, $v_2 = 40$ and $q = 3$. The Fourier domain under-sampled k-space is then converted into an MR image by taking the 2D-IDFT. This transformation reveals the coherent aliasing and Gibb's artifacts [1, 6]. The image is then re-shaped into a vector $\boldsymbol{f}^{'}$ prior to being fully sampled using a random Gaussian matrix $\boldsymbol{\Phi}$ to yield a measurement vector $\boldsymbol{y}^{'}$ as follows;

$$\boldsymbol{y}' = \boldsymbol{\Phi f}' \quad (15)$$

This random sampling converts the coherent artifacts in $\boldsymbol{f}^{'}$ into incoherent noise which is easier to denoise [6]. It also enables unique CS recovery in the DWT domain [4].

Next, the MR image is reconstructed from $\boldsymbol{y}^{'}$ in the DWT domain using the OMP method. This step compressively reconstructs the rows of $\boldsymbol{S}(u,v)$ that were not captured in $\boldsymbol{S_u^{'}}(u,v)$ during under-sampling [1, 5, 6]. The image is then converted into its k-space $\boldsymbol{S}^{''}(u,v)$ by determining the 2D-DFT. To reduce the artifacts and noise further, the non-zero k-space rows of $\boldsymbol{S_u^{'}}(u,v)$ that were captured in the first step of the algorithm are now inserted in $\boldsymbol{S}^{''}(u,v)$ to replace their corresponding CS reconstructed noisy rows to yield the output image k-space, $\boldsymbol{S_o}(u,v)$.

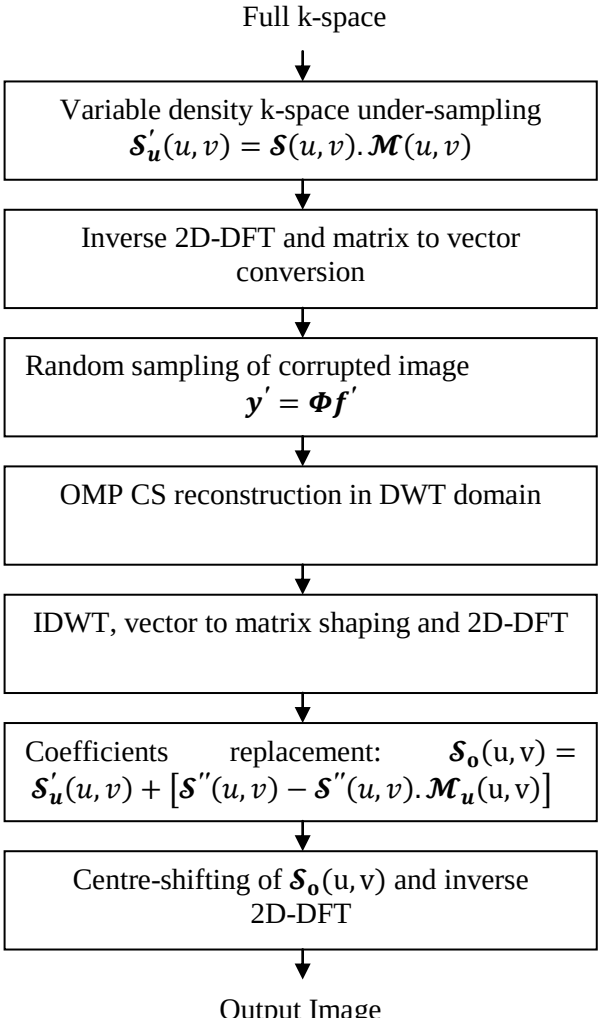

Fig.1. Block diagram of the proposed algorithm.

The rows substitution is accomplished as follows;

$$\boldsymbol{S_o}(u,v) = \boldsymbol{S_u^{'}}(u,v) + [\boldsymbol{S}^{''}(u,v) - \boldsymbol{S}^{''}(u,v).\boldsymbol{\mathcal{M}_u}(\mathrm{u,v})] \quad (16)$$

where $\boldsymbol{\mathcal{M}_u}(u,v)$ is a mask that is complementary to $\boldsymbol{\mathcal{M}}(u,v)$ and given by;

$$\boldsymbol{\mathcal{M}_u}(\mathrm{u,v}) = \mathrm{ones}(N_p\,, N_r) - \boldsymbol{\mathcal{M}}(\mathrm{u,v}) \quad (17)$$

where $\boldsymbol{S}^{''}(u,v).\boldsymbol{\mathcal{M}_u}(\mathrm{u,v})$ is the element-wise multiplication of $\boldsymbol{S}^{''}(u,v)$ by $\boldsymbol{\mathcal{M}_u}(\mathrm{u,v})$. Finally, the reconstructed image is generated by evaluating the 2D-IDFT of $\boldsymbol{S_o}(u,v)$.

To test the proposed method using MATLAB simulation, ground-truth MR images were converted into full k-spaces by taking the 2D-DFTs which were then subjected to the proposed algorithm.

4 Results and Discussions

To demonstrate the effectiveness of the proposed algorithm, MATLAB simulation results of thirty two images obtained from the MR image databases in [16-18] are presented here. All the images were first re-sized using bicubic interpolation prior to cropping them to a size of 64×32 pixels in order to use a sampling mask of the same size for all the images. The PSNR and SSIM metrics are used to assess the image reconstructed quality [1, 15].

In part (a) of fig. 2, a 64×32 pixels portion of a sagittal cross-section of a head ground-truth MR image is presented. An under-sampling mask that picks approximately 40% (26 rows) of the k-space is shown in part (b). The image reconstructed from the under-sampled k-space using the OMP method is presented in parts (c) and has a PSNR of 23.03 dB.
The image shown in part (d) was reconstructed using the proposed method. This image has a PSNR of 24.80 dB and is therefore of a better quality than the OMP reconstructed one.
Fig. 3 illustrates the stages of the proposed method using 50% measurements. Row (a) shows a 64×32 pixels ground-truth image for a portion of the pelvis and its full k-space matrix. At the left of row (b), the image reconstructed from the under-sampled k-space is presented. This image is corrupted by coherent artifacts and has a PSNR of 25.28 dB. The under-sampled k-space matrix is shown on the right of this image. The image reconstructed from the randomly sampled version of the image in part (b) using the OMP method is shown in part (c) together with its k-space. This image has a PSNR of 27.13 dB and exhibits high-frequency artifacts as is evident from a comparison of the k-spaces in parts (a) and (c). After re-insertion of the directly measured coefficients into the k-space of the image in part (c), the proposed method produces an image whose PSNR is 28.65 dB. This image plus the k-space matrix are presented in part (d). Inclusion of the coefficients re-insertion stage in the proposed method leads to an image quality which is better than that of conventional OMP.

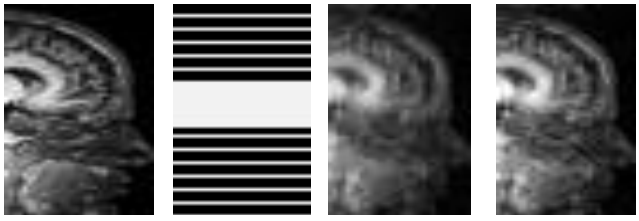

(a) (b) (c) (d)

Fig. 2. Comparison of the OMP and the proposed CS methods. (a) Ground-truth image. (b) A 40% sampling mask. (c) The OMP reconstructed image. (d) Image reconstructed using the proposed method.

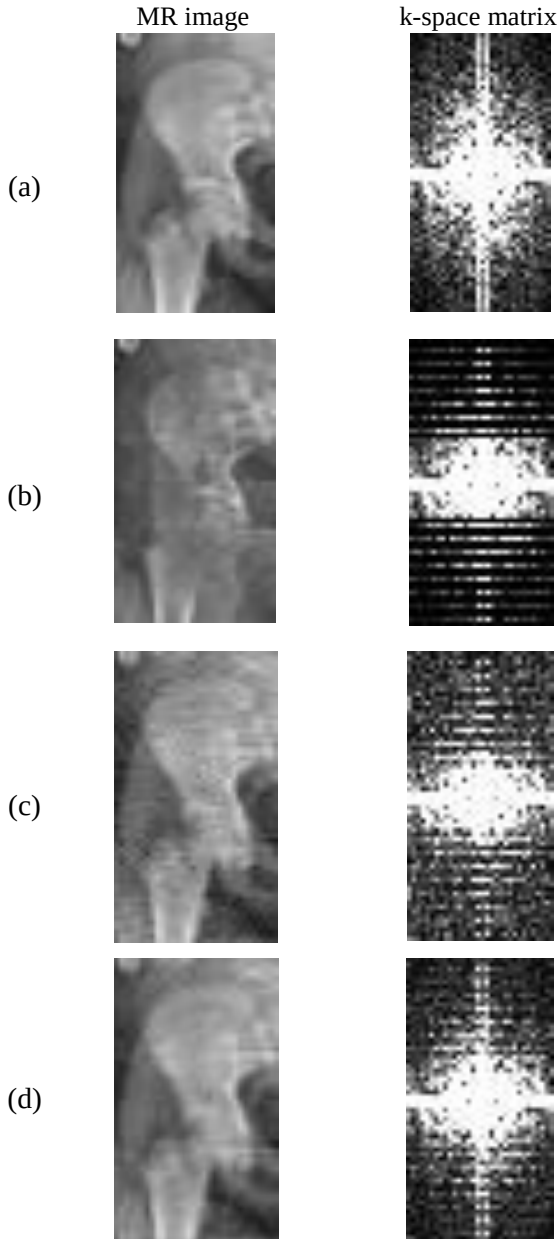

Fig. 3. Illustration of the proposed method. (a) Ground-truth image and k-space. (b) Under-sampled image and k-space. (c) OMP recovered image and k-space. (d) Proposed method recovered image and k-space.

Two MR images reconstructed using different CS methods at 40% measurements are shown in Fig. 4. The first row (a) shows the ground-truth images of blood vessels as well as a torso. Rows (b), (c) and (d) show the images reconstructed using the OMP, LASSO and the proposed methods respectively. The images reconstructed using the proposed method reveal the details better than those recovered using the other two methods.
In Table 1, the results of reconstruction of a thigh and a brain slice MR images using the proposed method and the LASSO method are shown. The k-spaces of the images were under-sampled at various percentage measurements.

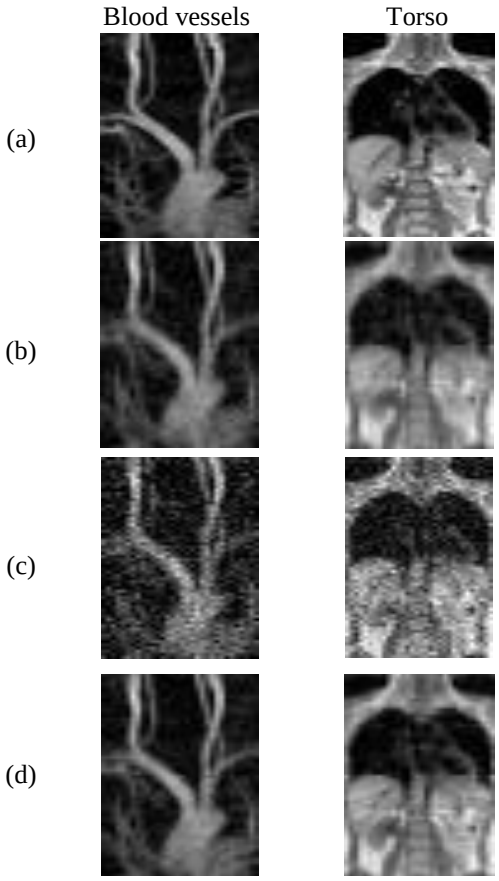

Fig. 4. Comparison. (a) Ground-truth MR image. (b) The OMP reconstruction. (c) The LASSO reconstruction. (d) Proposed method recovery.

The second-left column of the table presents the size of the measurement vector as a percentage of the image size. The third and fourth columns show the SSIM values of the reconstructed images using the LASSO and the proposed method respectively. The results show that the proposed method produced output images with higher SSIM index values than the LASSO optimization method for all the percentage measurements. Using the PSNR quality assessment index, similar results to those presented in table 1 were obtained. These results are as summarized in table 2. In the first column from the left, two ground-truth images are presented. They are images of parts of the pelvic bone and a shoulder. The second-left column presents the percentage measurements used. The third and fourth columns show the PSNR values of the images reconstructed using the OMP and the proposed methods respectively. From the table it is evident that the proposed method performs better than the OMP method. For example, at 30% measurements, the proposed method yields approximately 1.71 dB and 1.45 dB PSNR improvements over the OMP method for the pelvic bone and shoulder images respectively.

Table 1. The SSIM results of a thigh and a brain slice MR images

Input Image	Percentage Measurements (%)	LASSO SSIM	Proposed SSIM
	10	0.72	0.88
	20	0.81	0.95
	30	0.85	0.97
	40	0.85	0.98
	50	0.87	0.99
	60	0.89	0.99
	70	0.92	1.00
	10	0.61	0.81
	20	0.71	0.91
	30	0.77	0.94
	40	0.84	0.96
	50	0.85	0.97
	60	0.89	0.98
	70	0.90	0.99

Table 2. PSNR results for a pelvis and a shoulder images

MR Image	Percentage Measurements (%)	OMP PSNR(dB)	Proposed PSNR(dB)
	10	21.50	23.82
	20	25.88	26.47
	30	26.78	28.49
	40	27.50	29.28
	50	28.18	29.91
	60	28.81	30.41
	70	29.62	31.00
	10	16.32	17.83
	20	19.58	20.12
	30	19.97	21.42
	40	20.38	22.64
	50	23.73	25.65
	60	26.49	28.74
	70	28.37	30.04

A summary of the mean PSNR of the images reconstructed using three CS methods is presented graphically in part (a) of fig. 5. The proposed method produces images of higher quality than both the LASSO and OMP methods for all measurements. The average quality improvement of the proposed method at 30% or more measurements is 1.76 dB above the OMP method. This improvement translates to a 13% reduction in the scan-time for a given quality compared to the OMP method. For example, to reconstruct an image with a PSNR of 24.34 dB, the proposed algorithm and the OMP method require 30% and 43% of the full k-space respectively. In part (b) of fig. 5, the variance of the PSNR of the recovered images is presented. This summary shows that the proposed method has better reconstruction consistency than the other two. Similar results were obtained using the SSIM index.

(a)

(b)

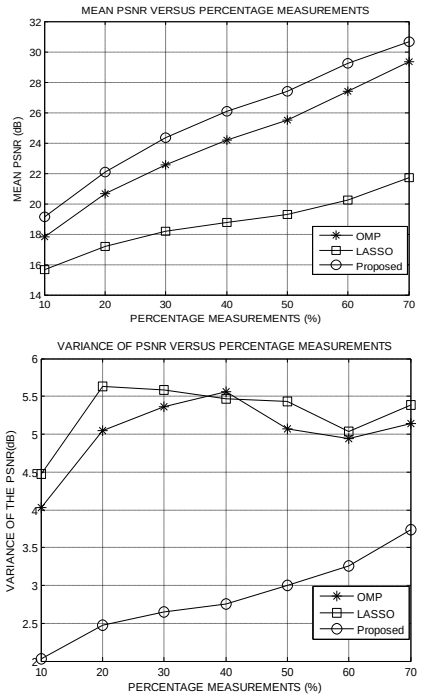

Fig. 5. Statistical summary. (a) Mean of PSNR. (b) Variance of PSNR.

5 Conclusion

A proposed CS-MRI algorithm has been presented in this paper. The algorithm reduces the imaging scan time by applying a variable-density k-space under-sampling technique. Substitution of some of the reconstructed k-space coefficients with the sampled ones was employed to improve the signal quality. Experimental results have been used to demonstrate that the proposed method reduces the MRI scan-time by 13 % compared to the OMP CS method. It also improves the image quality by an average PSNR of 1.76 dB for a given percentage measurement. Future work will focus on improving the under-sampling mask as well as the k-space substitution process.

References:

[1]Kiragu H, Mwangi E, Kamucha G. A Robust Compressive Sampling Method for MR Images Based on Partial Scanning and Apodization. *Proceedings of the IEEE ISSPIT*, Louisvlle, Kentucky, USA; Dec. 2018.

[2]Gnana F, John P, Sankararajan R. Efficient Reconstruction of Compressively Sensed Images and Videos Using Non-Iterative Method. *AEU-Intl. Journal of Electronics and Comm.*, Vol. 73, 2017, pp. 89-97.

[3]Jiang T, Zhang X, Li Y. Bayesian Compressive Sensing Using Reweighted Laplace Priors. *AEU-Intl. Journal of Electronics and Comm.*, Vol. 97, 2018, pp. 178-184.

[4]Yonina C. E, Kutyniok G. *Compressed sensing theory and applications*. 1st ed. Cambridge University Press, UK, 2015.

[5]Lustig M. *Sparse MRI*. PhD thesis. Stanford University, CA, USA, 2008.

[6]Vasanawala S. S, Alley M, Barth R, Hargreaves B, Pauly J, Lustig M. Faster Pediatric MRI via Compressed Sensing. *Proceedings on Annual Meeting of the SPR*, CA, USA; April 2009.

[7]Eslahi S. V, Dhulipala P. V, Shi C, Xie G, Ji J. X. Parallel Compressive Sensing in a Hybrid Space: Application in Interventional MRI. *Proc. of the Annual Intl. Conference of the IEEE EMBC*, Jeju Island, South Korea; July 2017.

[8]Kiragu H, Mwangi E, Kamucha G. A Hybrid MRI Method Based on Denoised CS and Detection of Dominant Coefficients. *Proc. of Intl. DSP conference*, London, UK; Aug. 2017.

[9]Mitra D, Zanddizari H, Rajan S. Improvement of Recovery in Segmentation-Based Parallel Compressive Sensing. *Proceedings of the IEEE ISSPIT*, Louisville, Kentucky, USA; Dec. 2018.

[10]Qin J, Guo W. An Efficient Compressive Sensing MR Image Reconstruction Scheme. *IEEE 10th Intl. Symp. Biomedical Imag.: nano to macro*, San Francisco, CA, USA; April 2013.

[11]Miyoshi T, Okuda M. Performance Comparison of MRI Restoration Methods with Low-Rank Priors. *Proceedings of the 7th IEEE GCCE*, Nara, Japan; Oct. 2018.

[12]Chun-Shien L, Hung-Wei C. Compressive Image Sensing for Fast Recovery From Limited Samples: A Variation on CS, *Elsevier Journal of Information Sciences*, Vol. 325, 2015, pp. 33–47.

[13]Nishimura D. G. *Principles of Magnetic Resonance Imaging*. Stanford University Press, USA, 2010.

[14]Hashemi R. H, Bradley W. G, Lisanti C. J. *MRI the Basics*. 3rd ed. Philadelphia: Lippincott Williams & Wilkins, USA, 2010.

[15]Wang, Z, Bovik, C. A universal image quality index, *IEEE Signal Proc. Letters*, Vol. 9, No. 3, 2002, pp. 81–84.

[16]Siemens Healthineers, *Dicom Images*, https:// www.healthcare.siemens.com/magnetic-resonance- imaging [Dec. 2018].

[17]Brown University, Rhode Island, USA. *MRI Research Facility*, https://www.brown. edu/ research/facilities/mri/, [Oct. 2018].

[18]Oregon Health and Science University, USA, *Diagnostic radiology*, https://www.ohsu.edu/xd/ education/schools/ school-of-medicine, [Sep. 2018].